Available online at www.sciencedirect.com
SCIENCE DIRECT®
Nuclear Physics A 741 (2004) 3–28
NUCLEAR PHYSICS A
www.elsevier.com/locate/npe

# Spectral statistics and the fine structure of the electric pygmy dipole resonance in $N = 82$ nuclei ☆

J. Enders [a], T. Guhr [b], A. Heine [a], P. von Neumann-Cosel [a], V.Yu. Ponomarev [a,1], A. Richter [a,*], J. Wambach [a]

[a] *Institut für Kernphysik, Technische Universität Darmstadt, D-64289 Darmstadt, Germany*
[b] *Matematisk Fysik, LTH, Lunds Universitet, Box 118, SE-22100 Lund, Sweden*

Received 22 December 2003; received in revised form 12 May 2004; accepted 14 May 2004

Available online 1 June 2004

**Abstract**

We study the statistical properties of the electric pygmy dipole resonance in four different isotones with neutron number $N = 82$. These nuclei are $^{138}_{56}$Ba, $^{140}_{58}$Ce, $^{142}_{60}$Nd, $^{144}_{62}$Sm. The data set comprises 184 levels with spin and parity $J^\pi = 1^-$ and their ground state $B$(E1) transition strengths. The statistics are found to be "mixed", i.e., in between the predictions of random matrix theory for correlated and uncorrelated spectra. Moreover, we calculate spectra and transition strengths in the quasiparticle phonon model (QPM). We compare experimental and theoretical findings. The incompleteness of the data sets and its impact on the results is discussed. A consistent picture emerges which yields an improved understanding of the statistical properties of the pygmy resonance.


*PACS:* 24.60.Lz; 21.10.-k

*Keywords:* NUCLEAR STRUCTURE $^{138}$Ba, $^{140}$Ce, $^{142}$Nd, $^{144}$Sm; Analyzed electric pygmy dipole resonance strength distributions, level density; deduced statistical properties. Quasiparticle phonon model calculations

☆ Work supported by Deutsche Forschungsgemeinschaft within the SFB 634 and by Det Svenska Vetenskapsrådet.
* Corresponding author.
*E-mail address:* richter@ikp.tu-darmstadt.de (A. Richter).
[1] Permanent address: Joint Institute for Nuclear Research, Dubna, Russia.

0375-9474/$ – see front matter 
doi:10.1016/j.nuclphysa.2004.05.014

## 1. Introduction

Low-energy electric dipole strength concentrated around 5–7 MeV in stable heavy nuclei has been studied for a long time [1], but its nature and systematic features remain a subject of discussion. This strength is commonly termed pygmy dipole resonance (PDR) since it is small compared to the E1 strength in the excitation energy region of the isovector giant dipole resonance (GDR). Most of the hitherto existing experimental information is restricted to gross properties of the mode, but the variation of its width, total strength and centroid energy are poorly understood.

Beyond resolving the long-standing problem of its structure, clarifying the nature of the PDR is important for a further number of reasons. Strongly excited soft E1 modes have also been observed in exotic, very neutron-rich isotopes (see, e.g., [2–4]), and it is an obvious question whether the underlying mechanism generating these modes is the same as for nuclei close to and in the valley of stability. Furthermore, the PDR is typically located close to particle threshold. This has important astrophysical implications because the thermal equilibrium of $(\gamma, n)$ and $(n, \gamma)$ reactions in explosive nucleosynthesis scenarios [5,6] can be considerably modified. Finally, since the low-lying E1 strength significantly influences the nuclear dipole polarizability through the inversely energy-weighted sum rule [7], its particular nature must be understood quantitatively.

A variety of models—with partly conflicting conclusions—exists for a theoretical interpretation of the PDR, ranging from hydrodynamical descriptions [8,9], neutron excess surface density oscillations [10–12], fluid-dynamical approaches [13–15] to local isospin breaking in heavy nuclei by clustering [16]. Microscopically, non-relativistic [17,18] and relativistic [19–21] random phase approximation (RPA) calculations predict a sizeable isoscalar E1 mode well below the GDR. Fragmentation of the E1 strength in the region of the PDR due to the coupling to complex configurations has been studied in [22–26].

Recently, important experimental progress has been made by high-resolution measurements of the fine structure of the PDR at various shell closures [22,27,28] using the nuclear resonance fluorescence technique. For the case of $^{208}$Pb, the comparison of experimental results and model calculations suggests [22] that the mode is due to surface neutron density vibrations, but some features of the low-energy E1 response seem also to be determined by transverse excitations characterized by toroidal transition current distributions [29].

Here, we pursue an alternative approach to shed light on the nature of the PDR. We investigate its statistical properties by employing random matrix theory (RMT). This theory, originally developed by Wigner and Dyson, is capable of describing spectral statistics in a unifying way for a rich variety of systems (for a review see [30]). In nuclear physics, a number of studies (see, e.g., [30–36]) address the question what kind of statistics is to be expected in different regions of the spectra. Roughly speaking, one can distinguish correlated, uncorrelated, and mixed behavior, depending on the excitation energy, mass number and on collective or single-particle character. Even though the complexity of the nuclear many-body problem does not always allow for an easy interpretation of the findings, general trends could be identified.

In a recent study, it was possible to draw conclusions from the spectral statistics on features of a particular excitation mechanism [35]. This investigation was concerned with $J^\pi = 1^+$ states excited by the orbital magnetic dipole scissors mode. The present

work builds upon the insights gained in [35]. Here, we focus on the PDR in four stable $N = 82$ semimagic nuclei. Recent experiments [28,37] provide a large data ensemble on the energies of $J^\pi = 1^-$ states and their ground-state transition strengths. However, both data sets are still incomplete because of limited experimental sensitivity with respect to the detection of weak transitions. On the other hand, fairly complete theoretical calculations, which should be compared to the data, are available within the microscopic quasiparticle phonon model (QPM) which provides a successful description of the PDR in $^{208}$Pb.

Statistical analysis of nuclear data is generally hampered by the problem of missing levels. This is so because the number of levels accessible in an experiment is lower than and the resolution is not as good as, e.g., in laser spectroscopic measurements for atoms and molecules. In $\gamma$ spectroscopic studies on excited heavy nuclei there is always a finite detector threshold, and individual transitions sometimes cannot be resolved experimentally. Thus, the present example is intended to serve as a model study. We show how to combine experimental and theoretical information to still obtain a consistent interpretation of the statistical measures for a specific excitation mode.

The paper is organized as follows. In Sections 2 and 3, respectively, the experimental data and the model calculations are briefly sketched. In Section 4, we extract statistical measures for the individual nuclei from the experimental and the theoretical data and compare them with RMT predictions. In Section 5 we construct and analyse a data ensemble by combining the data for all four nuclei. We discuss our results in Section 6 and conclude in Section 7.

## 2. Experimental data

From recent high-resolution photon scattering experiments [28,37] at the bremsstrahlung facility [38] of the superconducting Darmstadt electron linear accelerator S-DALINAC [39], a large data set on E1 excitations in $N = 82$ nuclei has been compiled. The data, totalling 184 excited $J^\pi = 1^-$ states with excitation energies and $B$(E1) excitation strengths, consist of 70 excitations in $^{138}$Ba, 48 excitations in $^{140}$Ce, 30 excitations in $^{142}$Nd, and 36 excitations in $^{144}$Sm. An overview over the experimental $B$(E1) strength distributions is shown in Fig. 1. This data set will serve as the data base for statistical analyses of the spectral correlations and strengths distributions. As can be seen from the figure, there is a clear concentration of $B$(E1) strength below the particle threshold which represents the PDR in these $N = 82$ nuclei. The lowest E1 excitation in each nucleus at energies between 3 and 4 MeV is known to be a two-phonon $1^-$ state which arises due to the coupling of the low-lying collective quadrupole and octupole vibrations [40]. Because of its particular regular collective structure, this E1 excitation has been left out in the following analyses and is not included in the level numbers given above.

Due to limited statistics and a non-resonant physical background in the spectra, there is a finite detection limit below which excitations cannot be observed. For experiments at the S-DALINAC, the detection threshold (while being generally energy-dependent) turns out to be flat over a wide energy interval so that a constant cut-off represents a good approximation. The value of the detection threshold for a given E1 transition has been $B_{\mathrm{th}}(\mathrm{E1}) \approx 1 \times 10^{-3}\,\mathrm{e}^2\,\mathrm{fm}^2$.

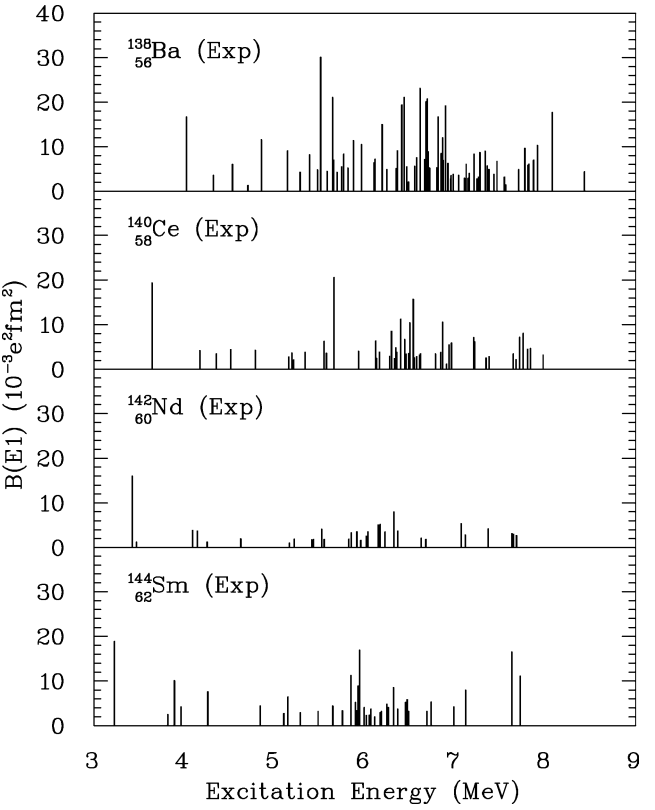


Fig. 1. Experimental strengths versus energy for the four $N = 82$ nuclei studied (data from [28,37]).

In order to understand one further property of the detection limit present in the experiments, we recall that the experimental signal in photon scattering experiments [41,42] is proportional to the energy-integrated cross section

$$I_f = \pi^2 \left(\frac{\hbar c}{E_x}\right)^2 \frac{2J+1}{2J_0+1} \frac{\Gamma_0 \Gamma_f}{\Gamma} \tag{1}$$

for a specific decay branch into the final state $f$. The excitation energy of the excited level is denoted by $E_x$, $J$ and $J_0$ represent the angular momentum of the excited and the ground state (in our case 1 and 0), respectively, and $\Gamma_0$ and $\Gamma_f$ indicate the partial decay widths of the excited state into the ground state (0) and the final state ($f$). The total width $\Gamma$ is the sum of all partial widths. An unambiguous determination of the decay width $\Gamma_0$ and the transition strength $B$(E1) from $\Gamma_0$ is only possible if all decay branches are known. For the vast majority of the observed excitations, only one decay branch to the ground state has been observed, and for the further analysis thus $\Gamma = \Gamma_0$ is assumed. Other decay branches were included in the analysis only if they have been observed experimentally. Transitions to low-lying states as, e.g., the $2_1^+$ states can be observed quite sensitively, and fast decays to high-lying states are not very likely due to the low transition energies. Therefore, the

uncertainty of the dipole excitation strengths can be estimated to be only of the order of a few percent. For the simple, but very frequent case $\Gamma = \Gamma_0$, the $B(\mathrm{E1})$ values can be determined directly from the measured cross sections $I_0$ via

$$\frac{B(\mathrm{E1})}{[\mathrm{e}^2\,\mathrm{fm}^2]} = 2.486 \times 10^{-4} \frac{[\mathrm{MeV}]}{E_\mathrm{x}} \cdot \frac{I_0}{[\mathrm{eVb}]}. \tag{2}$$

The multipole order of the excitations has been determined to be 1 from angular distribution measurements. The photon scattering experiments at the S-DALINAC utilize unpolarized bremsstrahlung in the entrance channel so that a determination of the multipole character of the resonantly scattered photons is only possible using a Compton polarimeter [43]. However, the polarization sensitivity is very small above 4 MeV, and parity information for excited states is only available for some states in $^{138}$Ba from an earlier experiment using a composite Euroball-Cluster detector [24]. However, a photon scattering experiment at the HI$\gamma$S facility using linearly polarized photons in the entrance channel [44] has not only confirmed the results of [24] but has unambiguously shown that the majority of the states in $^{138}$Ba plotted in the upper part of Fig. 1 are indeed $J^\pi = 1^-$ states. Neither microscopic model calculations nor other experiments in this mass and energy region have revealed $M1$ strength, but it cannot be excluded that for a few very weak excitations the assignment E1 might be not correct. On the basis of the observations in $^{138}$Ba it is thus fairly safe, however, to assume that the electric dipole strength distribution shown for the other $N = 82$ nuclei $^{140}$Ce, $^{142}$Nd, and $^{144}$Sm is indeed predominantly of electric nature.

## 3. Quasiparticle phonon model calculations

We briefly discuss the salient features of the quasiparticle phonon model (QPM) [45]. The Hamiltonian of the model includes a mean field for protons and neutrons, monopole pairing, and the residual interaction in a separable form. At the first stage, the Hamiltonian is diagonalized within a set of two-quasiparticle, $2qp$, (or particle-hole) configurations in even-even nuclei. To this end, the quasiparticle RPA (QRPA) equations are solved. Solutions of these equations are referred to as phonons. They are treated as quasi-bosons with quantum numbers $\lambda^\pi$. Among them one finds collective phonons corresponding to collective low-lying states and giant resonances, and furthermore a large number of practically pure $2qp$ excitations.

At the second stage, the wave functions of the excited states are expanded in terms of all one-phonon states with the same $\lambda^\pi$ and of complex configurations. The latter are obtained by combining different one-phonon configurations $\lambda_1^{\pi_1}, \lambda_2^{\pi_2}, \ldots$, of fixed quantum numbers $\lambda^\pi$ giving the $n$-phonon components of the wave function, i.e. $[\lambda_1^{\pi_1} \otimes \lambda_2^{\pi_2} \otimes \cdots \otimes \lambda_n^{\pi_n}]_{\lambda^\pi}$. The model Hamiltonian is now diagonalized in the space of the one-phonon and the complex configurations. The diagonalization yields eigenenergies of excited states and the weights with which the different components of the configuration space contribute to the wave function of each eigenstate state.

Since the model Hamiltonian contains only one-body and two-body pieces and is already pre-diagonalized on the first stage, the couplings in the model space become

hierarchical, coupling one- and two-, two- and three-, etc. phonon configurations. The matrix elements of these couplings are calculated microscopically employing the internal fermion structure of the phonons and the nuclear Hamiltonian.

An important feature of the excitation process should be emphasized: the one-body operator of an external electromagnetic field leads from the ground state, which is a phonon vacuum, to an excited state exclusively via the one-phonon components of the wave functions. The matrix elements for direct excitation of two-phonon components from the ground state are about two orders of magnitude smaller as compared to the excitation of one-phonon components and can thus be neglected in the presence of one-phonon configurations. The only exception is the lowest $1^-_1$ state which is of almost pure two-phonon nature $[2^+_1 \otimes 3^-_1]_{1^-}$ and has been omitted from the analyses of experimental data.

If the calculation is performed within a sufficiently large configuration space, the density of complex configurations is much higher than the one-phonon ones. Accordingly, most of the excited states carry only a small fraction of one-phonon components in their excitation strength. In other words, the coupling to the complex configurations leads to the fragmentation of the electromagnetic strength of the QRPA calculation over many excited states.

In many cases it is sufficient to only work within the boson picture of the phonons, neglecting their internal fermion structure. This implies that the interactions between two- and two-, three- and three-, etc. phonon configurations are neglected since they arise from Pauli principle corrections. Such an approximation cannot be applied in our particular case, since it leads to large degeneracies which totally spoil the level statistics. For two- and two-phonon interaction we are able to account for such matrix elements and we therefore restrict the modelspace to one- and two-phonon states and diagonalize the Hamiltonian in this space.

In the actual calculations of the dipole strength distribution below the threshold in $N = 82$ isotones, we have included in our model space phonons with multipolarity and parity ranging from $1^\pm$ to $9^\pm$. A typical size of the configuration space up to 8.0 MeV is then about 300 states. The neglect of three and more phonon states implies that the results do not reflect the statistical properties of *all possible* excited states available in the examined energy interval. For the reasons given above, the electromagnetic spectrum is however well accounted for in the truncated model space, and we therefore expect that the resulting levels to have statistical properties close to those observed in the experimental $(\gamma, \gamma')$ studies. The model parameters for the calculations have been adjusted for the case of $^{138}$Ba following a well-established procedure (see, e.g., [46]) and the same single particle spectrum, strength of monopole pairing and residual interaction has been used for all nuclei. The only variable parameter was the strength of the isoscalar residual interaction for $\lambda^\pi = 1^-$ phonons which is needed to put the spurious isoscalar $1^-$ state exactly at zero energy in each nucleus.

The results for the $B$(E1) strength distribution for $1^-$ states below 8.5 MeV in the $N = 82$ isotones are presented in Fig. 2. Especially the dependence of the integrated electromagnetic strength in the studied energy region as function of the proton number is much weaker in these calculations than experimentally observed (see Fig. 1). Furthermore, the total strength seems to be shifted to higher energies compared to the experiment.

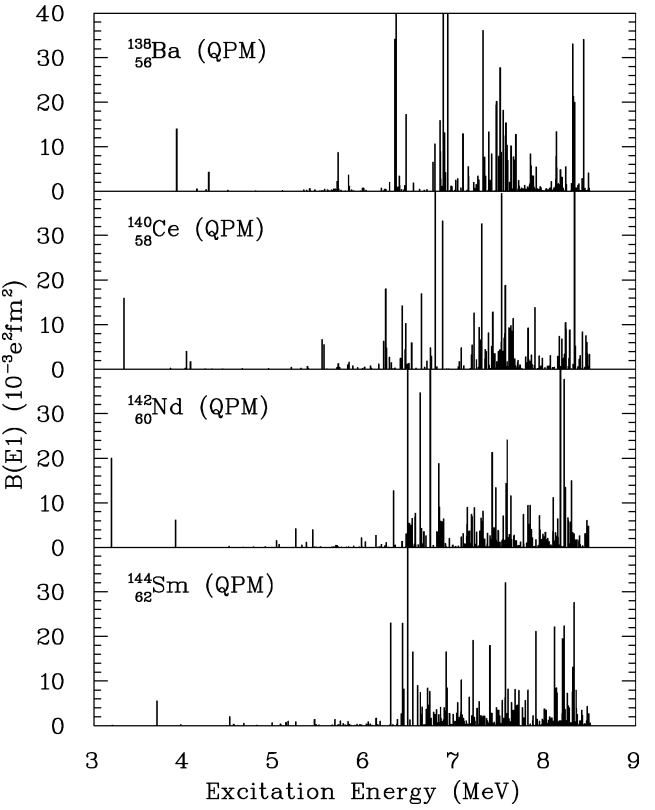


Fig. 2. QPM strengths versus energy for the four $N = 82$ nuclei studied.

For the subsequent statistical analysis we organize the theoretical spectra (Fig. 2) in two data sets:

- the full set of states ($\sim 300$) for the studied energy interval in each nucleus obtained within a complete one- and two-phonon basis,
- a subset of the states for which we cut away the weak transitions in such a way that the remaining numbers of transitions agree with those of the experiment. This cut-off is directly related to the experimental sensitivity limit. The latter data set will be refered to as "truncated QPM" and the weakest transitions included there are comparable in size to the experimental detection threshold of $10^{-3}$ e$^2$ fm$^2$ quoted above.

## 4. Statistical measures

After unfolding the data in Section 4.1, we work out the spacing distributions, the number variances and the strength distributions in Sections 4.2–4.4, respectively.

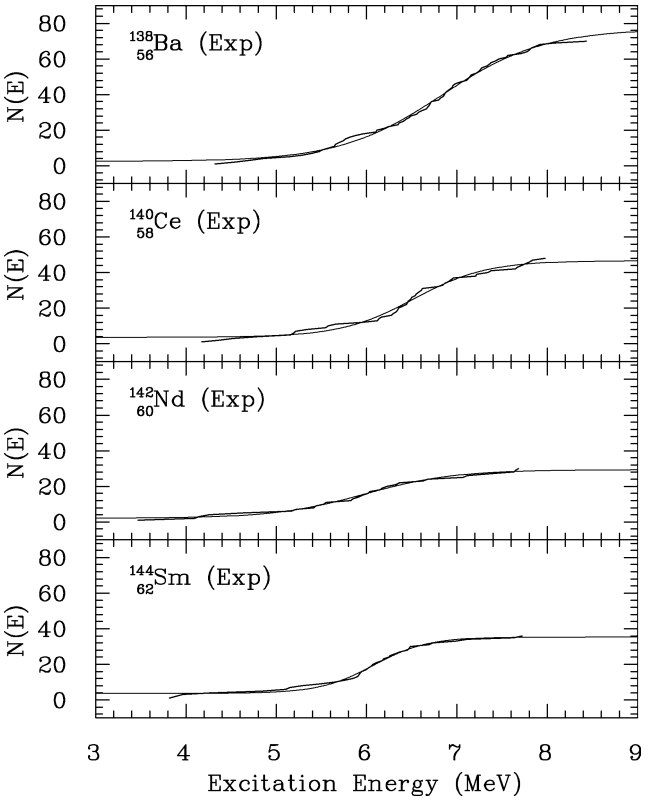


Fig. 3. Integrated level densities $N(E)$ together with a fit of the expression in Eq. (7) to the experimental data.

### *4.1. Unfolding the spectra and transition strengths*

To compare statistical properties of the experimental data with the predictions from random matrix theory [30,47–49] all effects due to the level density have to be removed properly from the experimental and theoretical data. This rescaling of the energy levels $E_i$, $i = 1, 2, 3, \ldots$ and the corresponding transition strengths $B_i(\mathrm{E1})$, $i = 1, 2, 3, \ldots$ is referred to as "unfolding". The stick spectrum or spectral function is obtained by putting a $\delta$ function at the position $E_i$ of every level. Its integral up to a certain energy $E$ is the staircase function (Figs. 3 and 4)

$$N(E) = \sum_i \Theta(E - E_i). \tag{3}$$

It is decomposed into an averaged, smooth part and a fluctuating part, $N(E) = N_{\mathrm{av}}(E) + N_{\mathrm{fluc}}(E)$, such that the integral of $N_{\mathrm{fluc}}(E)$ is zero. New, dimensionless energy variables are defined by

$$\epsilon_i = N_{\mathrm{av}}(E_i). \tag{4}$$

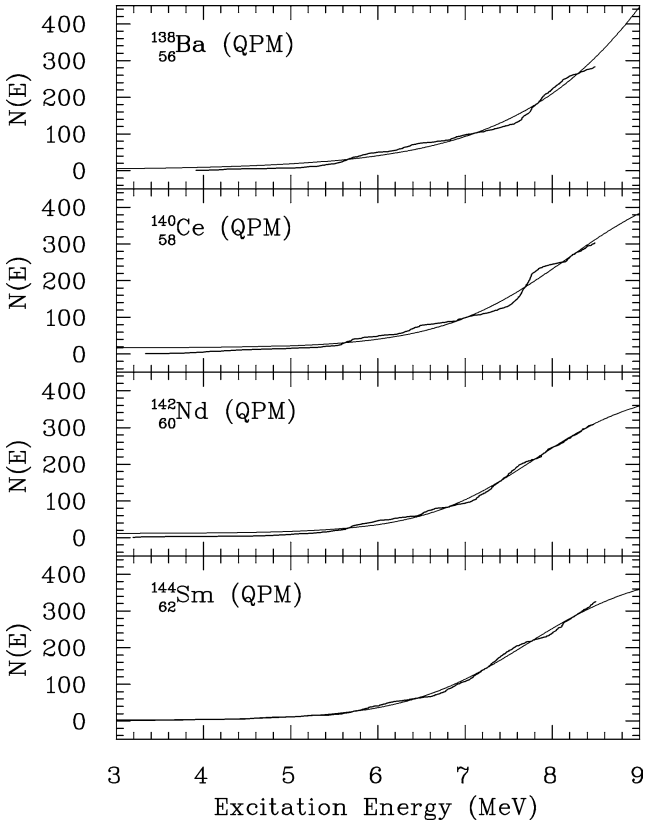


Fig. 4. Integrated level densities $N(E)$ together with a fit of the expression in Eq. (7) to the QPM data. The inflection point of the staircase function visible in Fig. 3 is shifted to the right here, i.e., to higher energies.

This mapping ensures that the level density in $\epsilon_i$, $i = 1, 2, 3, \ldots$ is a constant. If the total level number is sufficiently large and the fluctuating part $N_{\mathrm{fl}}(E)$ does not vary too strongly, the density of levels at the energies $\epsilon_i$ should be unity by construction. For our data this condition is not met. The level density in the $\epsilon_i$ will be a constant different from unity. This is so because for our data the quantity $N_{\mathrm{av}}(E)$ deviates significantly from $N(E)$ at the upper and lower ends of the spectrum and thus the difference between the largest unfolded level $\epsilon_{i_{\max}}$ and $\epsilon_1$ is different from $i_{\max} - 1$ as it should be for correct normalization of the spacings to unity. We will divide out this constant by hand to ensure the correct normalization. We emphasize that this adjustment does not change the correlation patterns, it simply puts them on the correct scale.

To unfold the transition strengths, we apply the procedure given in [50]. The measured transition strength in

$$y_i = \frac{B_i(\mathrm{E1})}{B_{\mathrm{av},i}(\mathrm{E1})} \tag{5}$$

is divided by a mean value which is obtained by the smoothing

$$B_{\mathrm{av},i}(\mathrm{E1}) = \frac{\sum_j B_j(\mathrm{E1}) \exp(-(\epsilon_i - \epsilon_j)^2/8)}{\sum_j \exp(-(\epsilon_i - \epsilon_j)^2/8)} \tag{6}$$

around the corresponding unfolded energy $\epsilon_i$. For further details, see the discussion in [50]. We notice that all transitions considered here are transitions to the ground state, as discussed above.

The crucial step in the unfolding is the appropriate determination of the averaged, smooth part $N_{\mathrm{av}}(E)$ of the staircase function. In many cases, such as the spectra of, e.g., microwave resonators [51] or molecules [52], one has some analytical understanding [53] of $N_{\mathrm{av}}(E)$, at least as far as the functional form is concerned. Unfortunately, information of this kind is lacking in the present case. However, we know that the $J^\pi = 1^-$ pygmy resonances exist only in a certain region of the spectrum, confined by a lower and an upper bound. This can be seen in Fig. 1. Thus, the level density of these states alone must exhibit a hump. Its integral, the corresponding staircase function, should have an inflection point. A convenient choice is the function

$$N_{\mathrm{av}}(E) = \frac{a}{1 + \exp((E-b)/c)} + d, \tag{7}$$

where $a$, $b$, $c$, and $d$ are fit parameters to be determined for every spectrum individually. All staircase functions, experimental and theoretical, are well described by this function. We notice that, in particular, polynomial fit functions give considerably less suitable fits. However, the results of Section 4 seem to be stable with respect to different unfolding procedures, unless the data are overfitted with functions containing too many parameters.

The experimental staircase functions together with the fit of Eq. (7) are shown in Figs. 3 (experiment) and 4 (QPM). A comparison of Figs. 3 and 4 shows that the experimental integrated level densities saturate in the measured excitation energy range, while the calculated ones still increase, with a slight indication of saturation at the highest energies. This is partly due to the fact that the energy centroid of the predicted $J^\pi = 1^-$ states is somewhat higher than that of the experimental ones.

### *4.2. Spacings distributions*

The nearest neighbor spacings distribution $P(s)$ measures the probability density to find two adjacent levels separated by a distance $s$ in the unfolded spectrum. In case of fully correlated energy levels, one expects the Wigner surmise

$$P(s) = \frac{\pi}{2} s \exp\left(-\frac{\pi}{4} s^2\right), \tag{8}$$

which reflects the repulsion of levels. On the other hand, if correlations are lacking completely, one should find the Poisson law,

$$P(s) = \exp(-s). \tag{9}$$

In random matrix theory, a system which is invariant under time reversal and free of Kramers degeneracies can be modeled by real symmetric matrices with random entries.

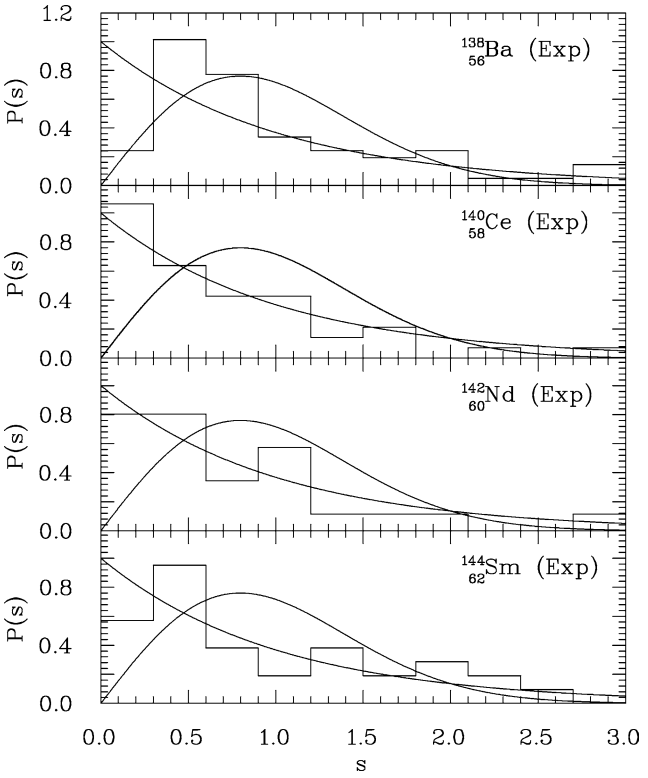


Fig. 5. Nearest neighbor spacings distributions for the four experimental spectra (histograms) compared to RMT predictions (solid lines) for a Poisson and a GOE behavior, respectively.

If no basis is distinguished, the correlations are at a maximum strength and one has the Gaussian orthogonal ensemble (GOE) of random matrices [30,47,49]. The corresponding spacing distribution is very close to the Wigner surmise. There are no correlations if the matrices are diagonal. This yields the Poisson law.

The nearest neighbor spacings distributions (NNSD) of the four experimental spectra are shown in Fig. 5. The statistics are in between the Wigner surmise and the Poisson law. This is referred to as intermediate or "mixed" statistics. While the distributions for Ce and Nd are very close to the Poisson law, Ba and Sm exhibit a certain degree of level repulsion. For the QPM the corresponding spacings distributions look rather similar, as displayed in Fig. 6. The case of Ce is still close to the Poisson law, while the other nuclei follow neither purely the Wigner surmise nor the Poisson law.

We have, however, to face the problem of missing levels in the experimental data. We expect that the truncation of the QPM data, as described in Section 3, models this effect at least qualitatively. The nearest neighbor spacings distributions for the truncated QPM spectra are also presented in Fig. 6. The distributions are moved closer towards the Poisson law. However, due to the relatively small level numbers, one cannot clearly decide

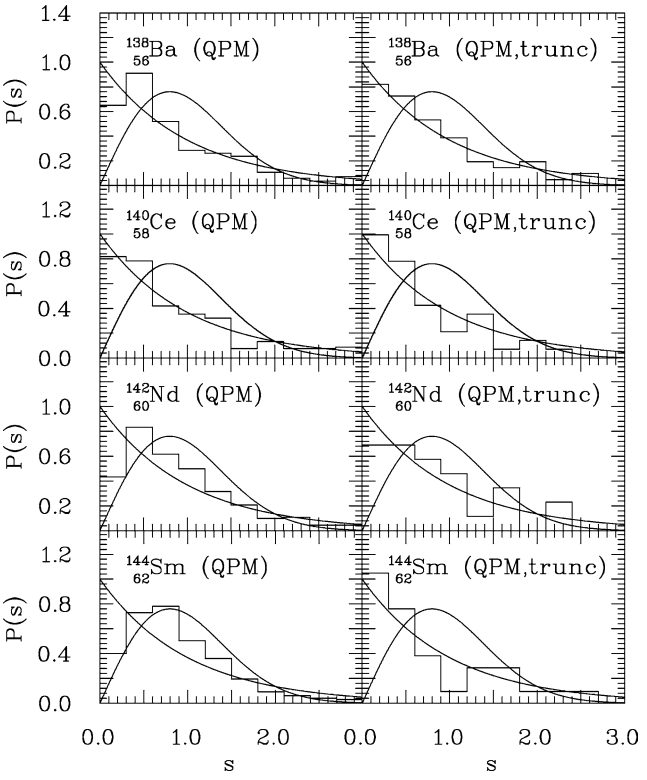


Fig. 6. Left: Nearest neighbor spacings distributions for the four QPM spectra showing similar properties as observed for the experimental data in Fig. 5. Right: Nearest neighbor spacings distributions for the four truncated QPM spectra.

which theoretical data set yields a better agreement with the experimentally found nearest neighbor spacings distributions.

Depending on the details of the dynamics, many possible scenarios exists for mixed systems. In the literature, one often employs the purely phenomenological Brody distribution [57]

$$P_\omega(s) = (1+\omega)\cdot\left[\Gamma\left(\frac{2+\omega}{1+\omega}\right)\right]^{1+\omega}\cdot s^{\omega}\exp\left\{-\left[\Gamma\left(\frac{2+\omega}{1+\omega}\right)\right]^{1+\omega}s^{1+\omega}\right\} \tag{10}$$

which interpolates between GOE or Wigner–Dyson statistics (8) (for $\omega = 1$) and Poisson statistics (9) (for $\omega = 0$). Values of the transition parameter $\omega$ between 0 and 1 correspond to mixed statistics. Fitting the Brody distribution to the data, we obtain values for $\omega$ as given in Table 1. However, one has to remark the following: the high complexity of the nuclear many-body problem leads to many different excitation modes, to a variety of collective, single-particle and even combined excitations. Purely collective ones are regular and thus give Poisson statistics. Nevertheless, in a more realistic description, the collective excitations are approximations to coherent single-particle motion. Thus, the fact that all excitations are ultimately rooted in single-particle motion couples all of them with

Table 1
Brody parameters $\omega$ for all spacings distributions discussed in this section

| | Experiment | QPM | Truncated QPM |
|---|---|---|---|
| $^{138}$Ba | 0.6 | 0.2 | 0.1 |
| $^{140}$Ce | 0.0 | 0.0 | 0.0 |
| $^{142}$Nd | 0.0 | 0.5 | 0.2 |
| $^{144}$Sm | 0.2 | 0.6 | 0.0 |

one another. In an appropriate energy basis, one could model that in terms of matrices assembled of several blocks, all coupled with one another. This would be similar to the models put forward by Bohigas et al. in [58]. The level statistics resulting from such a model would depend in a non-trivial way on several parameters characterizing these blocks. In summary, the Brody parameter is to coarse a measure and cannot give a deeper understanding for the complicated structure of the many-body system.

### *4.3. Number variances*

While the NNSD gives information about the level statistics on short scales of one or two mean level spacings, the level number variance $\Sigma^2(L)$ probes larger scales of $L$ mean level spacings. In the absence of correlations, one simply has $\Sigma^2(L) = L$, which is Poisson's error law. If GOE-type-of correlations are present, $\Sigma^2(L)$ is suppressed in an asymptotically logarithmic fashion [30,47,49]. As our spectra are relatively short, we can work out the level number variance only up to about $L = 6$.

The experimental level number variances $\Sigma^2(L)$ are shown in Fig. 7. The strongest spectral correlations are found for Ba and Nd. These nuclei yield level number variances closest to the GOE prediction. Remarkably, no correlations are seen for Ce where we find Poisson statistics. The nucleus Sm shows intermediate behavior. We notice that these findings are not in contradiction to those for the nearest neighbor spacings distributions. They yield additional information about larger scales in the spectra. The level number variances for the QPM are displayed in Fig. 8. A striking overshoot over the Poissonian behavior is seen. While the missing-level effect should lead to uncorrelated, i.e., Poissonian, behavior, the overshoot must be due to an additional clustering of states. Such a clustering occurs, e.g., when collective one-particle–one-hole states act as doorway states for more complex configurations. The QPM results can be interpreted in such a way and we return to this point later. The clustering effects, however, disappear in the truncated QPM, as shown in the right panel of Fig. 8. The level number variances now come closer to the Poissonian behavior.

A critical discussion addressing the role of the missing levels is in order. As is well known, even in cases where the fraction $f$ of observed transitions relative to all transitions is close to unity, sizeable deviations from the true correlation patterns for the complete spectra can be found. The truncation procedure applied above is probably a realistic way of taking the missing level effect into account. Various methods to estimate the observed fraction have been worked out for correlated sequences [54,55]. Unfortunately, we cannot utilize them fully as they are based on an assumption about the statistical fluctuation

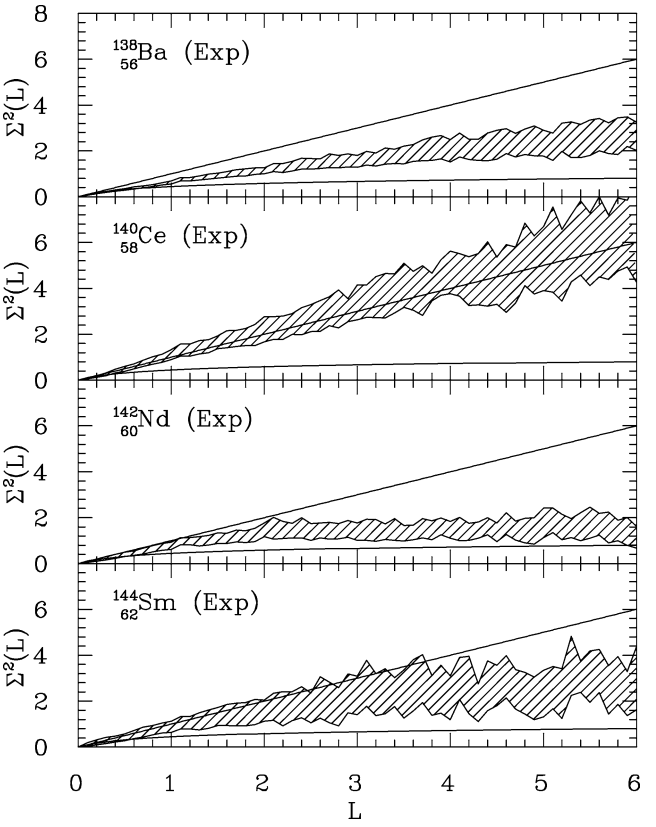


Fig. 7. Number variances with statistical uncertainty (plotted in form of an error band) for the experimental spectra compared to Poissonian respectively GOE behavior.

properties of the complete sequence. Determining these properties, however, is the aim of our work. We apply the expression derived in [55], that, in principle, allows one to estimate the observed fraction $f$ of a correlated sequence by fitting a theoretical result to the experimental number variances. Under the *assumption* that the complete sequence shows GOE behavior and that a fraction $f$ of the levels has been observed, the experimental number variance should be

$$\Sigma^2_{\mathrm{Exp}}(L) = (1-f)L + f^2\,\Sigma^2_{\mathrm{GOE}}(L/f). \tag{11}$$

Performing a fit of this expression in the interval $0 < L < 2$ to the experimental data, we obtain for the four nuclei $f_{\mathrm{Ba}} = 0.5$, $f_{\mathrm{Ce}} = 0.0$, $f_{\mathrm{Nd}} = 0.3$, and $f_{\mathrm{Sm}} = 0.2$. However, as Eq. (11) basically interpolates between the GOE and the Poisson prediction, the result of our fits simply reflect the fact that the experimentally found $\Sigma^2(L)$ shows some intermediate statistics in the case of Ba and is close to Poisson in the case of the other nuclei. But it should be stressed again that we do not know whether the underlying assumption, i.e., GOE behavior, is valid here.

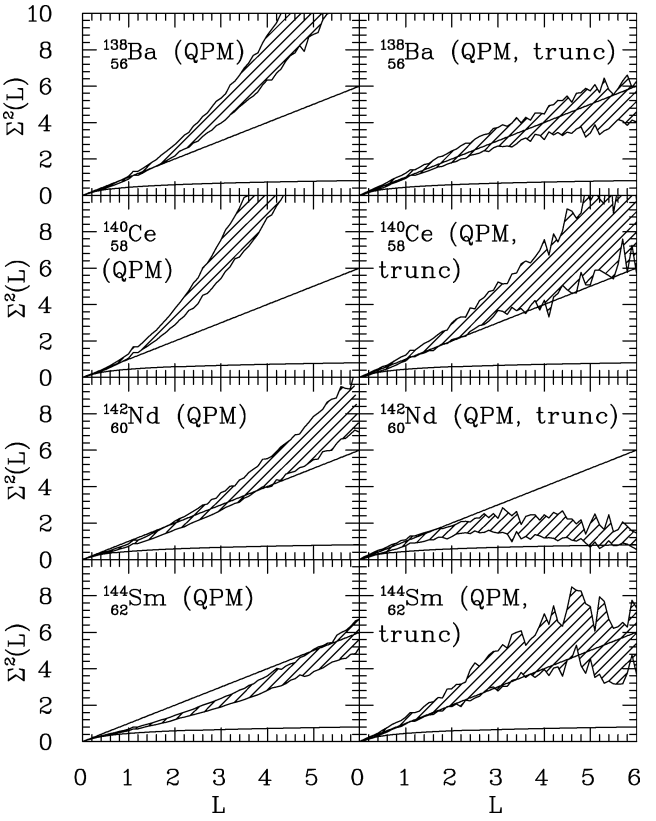


Fig. 8. Left: Number variances for the QPM data showing anti-correlations, which indicate a clustering of levels in the spectra. Right: The number variances for the truncated QPM are close to Poissonian behavior for all four nuclei.

### *4.4. Transition strength distributions*

Random matrix theory also makes a prediction about the wave function statistics. In the case of GOE correlations, the wave function components or, equivalently, their squares follow a Gaussian or Porter–Thomas distribution, respectively. In the Poisson case no unique statement can be made. In the trivial case of a diagonal random matrix, the wave functions are the Cartesian basis vectors and the distribution should consist of three sharp peaks at 0 and at $\pm 1$. However, the experiment yields no direct information about the wave function. One measures the transitions strengths. We follow the discussion in [56] to obtain a qualitative understanding of their distribution. The transitions strengths are the squares of the transition matrix elements. The latter read $\langle u_f|O(\mathrm{E1})|u_i\rangle$ where $u_i$ and $u_f$ are the initial and final states and $O(\mathrm{E1})$ is the transition operator. Representing $O(\mathrm{E1})$ by some fixed matrix in the random matrix model, one can work out the transitions strength distribution if the distribution of the wave functions components is known. Here, a line of arguing is used similar to the derivation of the central limit theorem. For large level number,

one expects asymptotically a Gaussian for the distribution of the transition matrix elements, if the distributions of the wave functions components have finite moments. However, for that conclusion to hold, the matrix representing the operator $O(\mathrm{E1})$ should have entries almost everywhere, i.e., it should not contain too many zeros. In any case, one sees that the distribution $P(y)$ of the normalized transition strengths $y$, as defined in Eq. (5), is of the Porter–Thomas type,

$$P(y) = \frac{1}{\sqrt{2\pi y}} \exp(-y/2), \tag{12}$$

if the distributions of the wave functions components is Gaussian. Moreover, it should approach this distribution more or less, even if the distribution of the wave function components is strongly non-Gaussian or even sharp. Thus, from the shape of the transition strength distribution, a clear conclusion about the spectral correlations cannot be drawn.

Nevertheless, an advantage of this distribution is that it is, statistically speaking, just a probability density and not a correlation function, implying that it is less sensitive to missing levels. As the loss of weak transitions typically corresponds to a random removal of levels from the spectra, it yields a certain truncation of the strengths distribution. This is easy to handle in the analyses, and one can estimate how the missing levels modify the theoretical distribution. If the transitions below a certain strength are not observed, the transition strength distribution reads [54,59]

$$P(y) = \begin{cases} 0, & y < y_0, \\ \frac{\exp(-y/2)}{\operatorname{erfc}(\sqrt{\frac{y_0}{2}})} \cdot \frac{1}{\sqrt{2\pi y}}, & y \geqslant y_0. \end{cases} \tag{13}$$

Here, $y$ and $y_0$ denote the strengths and the minimum observed strength in units of the mean *observed* strength,

$$y = \frac{B(\mathrm{E1})}{B_{\mathrm{av,obs}}(\mathrm{E1})} \quad \text{and} \quad y_0 = \frac{B_{\min}}{B_{\mathrm{av,obs}}(\mathrm{E1})}. \tag{14}$$

Both numbers can directly be deduced from the data sets. For $y_0 = 0$ one recovers the Porter–Thomas distribution. The observed fraction $f$ itself if given by the integral

$$f = \int_{y_0}^{\infty} P_{y_0=0}(y)\, dy. \tag{15}$$

For comparison with data it is useful to work out the distribution $P(z)$ for the logarithm

$$z = \log_{10} y \tag{16}$$

of the normalized strength, instead of the distribution $P(y)$ itself.

As a first step, we tested Eq. (13) and the loss of weak transitions with synthetic data. This is displayed in Fig. 9. We find that the model gives a good description of the truncation as long as the observed fraction $f$ is not too small. Fig. 10 shows the experimental strength distributions in comparison with the Porter–Thomas distribution (Eq. (12)) and its modification given by Eq. (13). In Fig. 11, one sees the transition strengths distributions for the full and the truncated QPM data, respectively. The truncation

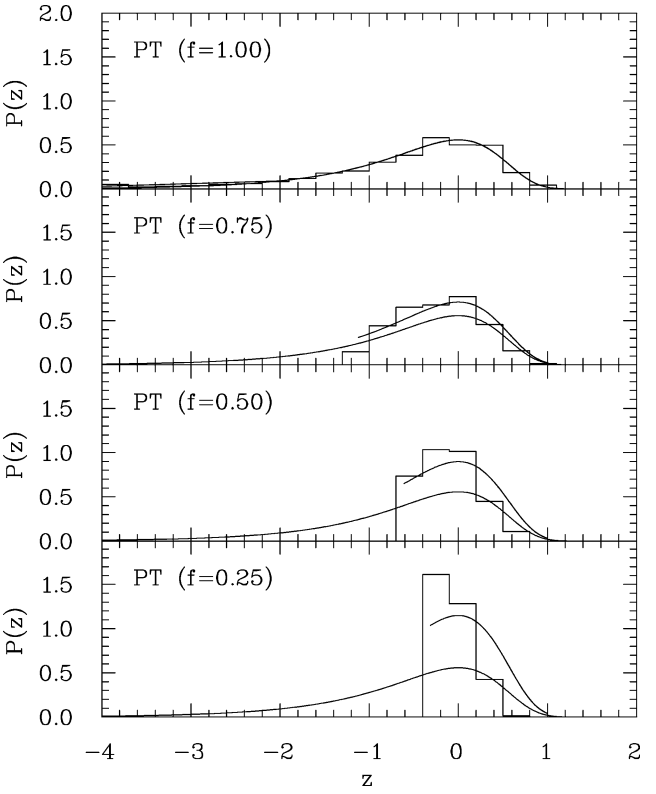


Fig. 9. Synthetic Porter–Thomas (PT) distributed data with different "observed fractions" $f$ of transitions (histograms) in comparison to the Porter–Thomas distribution and the modified Porter–Thomas distribution of Eq. (13). Note, that the curves of the modified Porter–Thomas distribution start at those values of $z$ that correspond to the smallest observed transition strength. For $f = 1.00$ the result of Eq. (13) is identical with the Porter–Thomas curve. For $f = 0.25$ one obtains a situation that resembles the experimental results (Fig. 10), indicating that in the experiment one indeed is dealing with incomplete sequences of $f \approx 0.1$.

of the QPM leads to strength distributions peaked similar to the experimental ones, as seen in Fig. 11. Importantly, these distributions are also similar to the ones in Fig. 9. However, we emphasize again that the occurrence of the Porter–Thomas distribution or distributions consistent with its truncated versions (13) for the transition strength does not directly indicate the presence or absence of correlations in the spectra.

## 5. Data ensemble

We use the data sets of the four individual nuclei discussed in Section 4 to construct a data ensemble. It contains 180 spacings originating from four spectra with 184 levels and 184 transition strengths for both the experiment and the truncated QPM. The full QPM data ensemble comprises about 1200 levels and strengths.

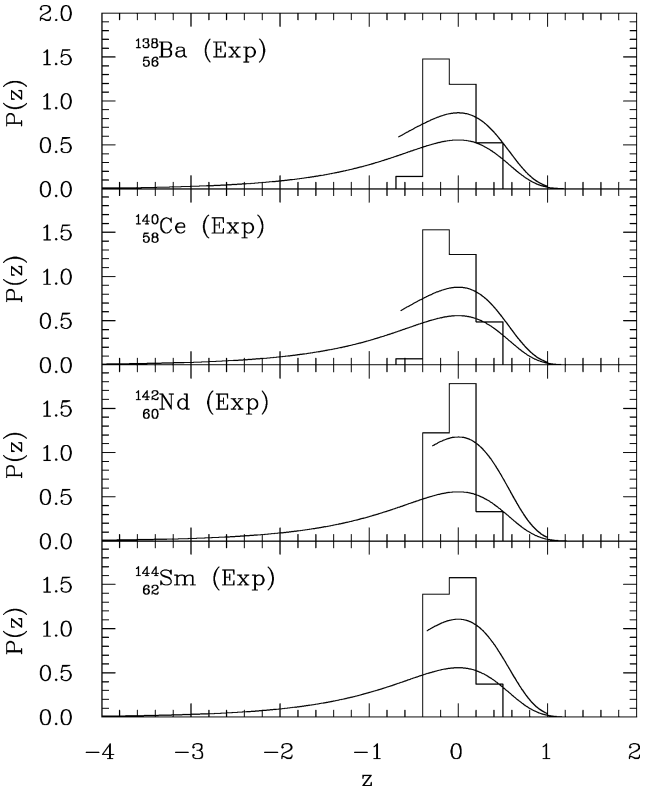


Fig. 10. Experimental strength distributions (histograms) together with a normal Porter–Thomas distribution and a distribution that describes the missing of the weak transition (Eq. (13)).

The NNSDs show similar behavior for experiment, QPM, and truncated QPM, as displayed in Fig. 12. In all cases the distribution is close to Poisson, with some remnants of level repulsion in the experiment and the full QPM. These remnants are mainly limited to a lowered probability in the first bin. The transition strength distribution is Porter–Thomas for the QPM and significantly deviates from Porter–Thomas in the experiment and for the truncated QPM data, as seen in Fig. 13. However, these deviations look rather similar. All in all, the truncation of the QPM leads to qualitative agreement with experiment. The spacing distribution for the data ensemble agrees slightly better with the result for the non-truncated QPM, but this could be a coincidence within the statistical significance of our analysis. For the transition strengths, qualitative agreement between calculation and experiment can be achieved by truncation of the weak states in the QPM data sets.

## 6. Discussion

The four $N = 82$ isotones individually and their combined data ensemble exhibit intermediate, i.e., “mixed”, spectral fluctuation properties in between GOE and Poisson

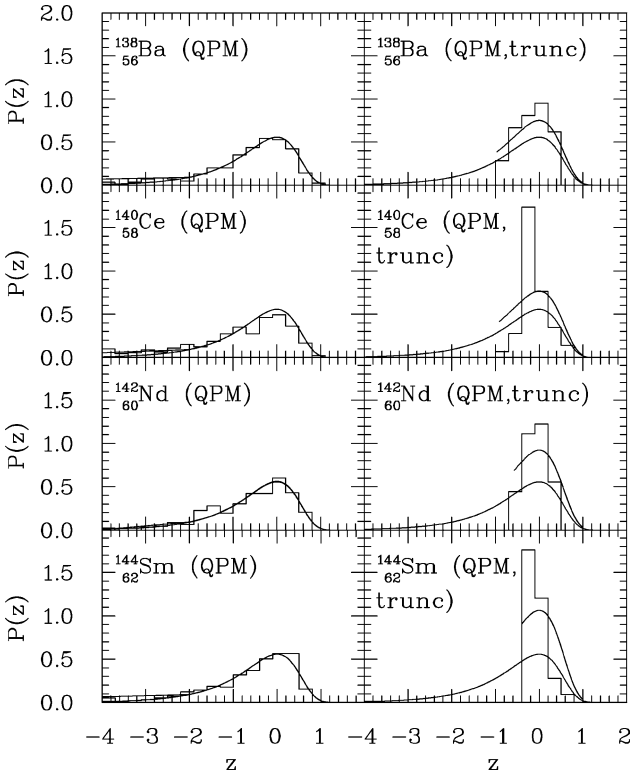


Fig. 11. Left: Strength distributions for the QPM results together with a Porter–Thomas distribution and a Porter–Thomas distribution modified to incorporate the missing of the weak transitions (Eq. (13)). These two curves (almost) perfectly coincide. Right: Strength distributions for the truncated QPM (histograms) together with a normal Porter–Thomas distribution and a modified one that describes the missing of the weak transitions (Eq. (13)).

statistics. Furthermore, all experimental transition strength distributions are quite different from Porter–Thomas. The full QPM data sets show strength distributions that are close to Porter–Thomas, i.e., GOE statistics, while their spectral statistics are still in between the Poisson and the GOE prediction. The statistics of the QPM calculation qualitatively match the experimental findings after properly truncating levels and strengths belonging to weak transitions. This truncation employs a realistic estimate for the experimental detection threshold. This illustrates the severeness of the missing level effect.

Importantly, the full, i.e., non-truncated, QPM data are incomplete, as well. This is because the present QPM calculation does not take in to account 3 and higher phonon configurations. Performing 3-phonon-QPM calculations one obtains about $10^3$ E1 transitions per nucleus. However, the statistical properties of these calculated transitions would be unrealistic, because it is prohibitively difficult to correctly include the interaction among the 3-phonon configurations. As the spectral correlations are most severely altered by missing a large fraction of levels, the truncation to a 2-phonon QPM does not affect the nearest neighbor spacings distribution significantly.

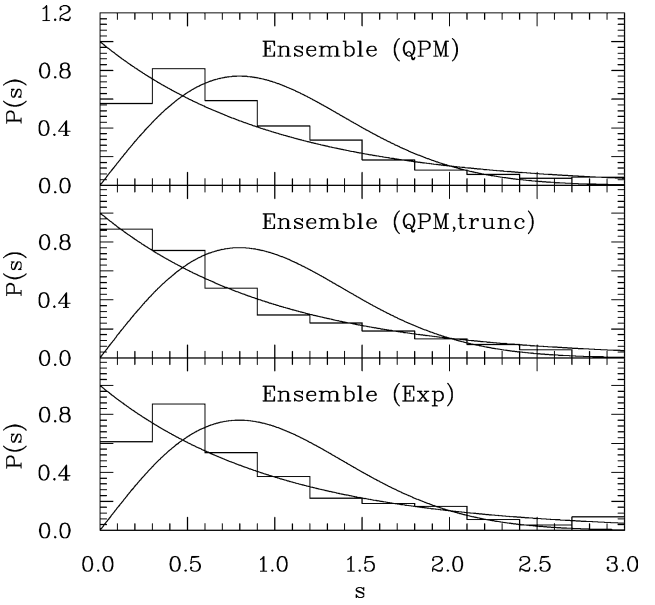


Fig. 12. Spacings distributions for the data ensemble constructed from all four nuclei. Experiment, QPM, and truncated QPM show a behavior that is close to Poisson (with some remnants of level repulsion in the experiment and the full QPM). The lack of spectral correlations indicates that the number of missing levels is large.

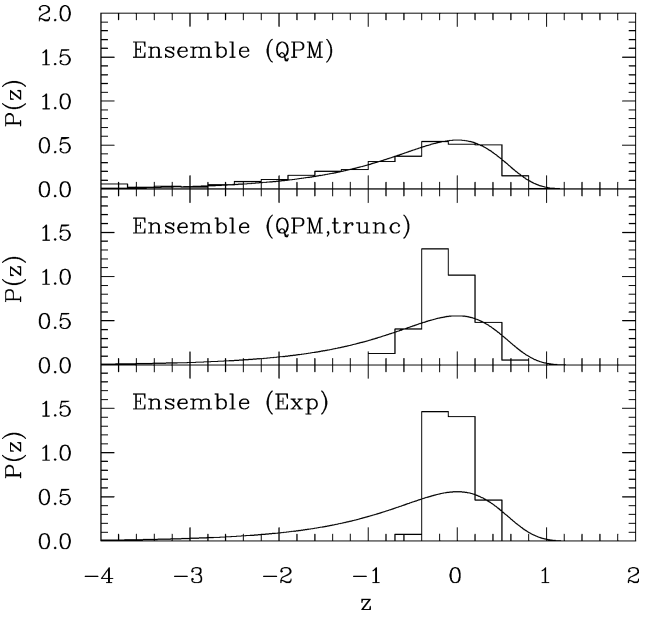


Fig. 13. Strength distributions for the data ensemble constructed from all four nuclei. The QPM spectrum shows good agreement with Porter–Thomas statistics, while experiment and truncated QPM deviate from the Porter–Thomas statistics, but in a similar way.

Since the level numbers are about 50 per nucleus in the experiment and about 300 in the QPM, we have to face the possibility that we see less than 10 percent of the transitions in the experiment and less than 30 percent in the QPM. Thus, all data sets analyzed here are incomplete. Nevertheless, the QPM calculation as performed, seems to properly match the experimental situation. This is borne out by the qualitative agreement between the experimental and the theoretical nearest neighbor spacings distribution.

A striking overshoot over the Poisson behavior is seen in the long-range statistical measures, i.e., in the level number variance for the full, non-truncated QPM data, as already mentioned above. Zooming into the QPM strength function versus energy in Fig. 14 helps to gain a qualitative understanding of this effect. One sees groups of states, clustered around a few states carrying large strength. These few states are those stemming from the first stage of the QPM calculation. At the second stage, they act like doorway states for the coupling to more complex configurations. This explains why Fig. 14 can be viewed as consisting of various superimposed Lorentzians around the few doorway states. The level density is influenced similarly. This leads to a bumpy structure on top of the averaged, smooth part $N_{\mathrm{av}}(E)$ of the staircase function and, thus, to the overshoot in the level number variance. To illustrate this, we consider a synthetically generated spectrum of uncorrelated levels whose level number variance is known to be $\Sigma^2(L) = L$. We now convolute it with a sum of Lorentzians whose widths is comparable to their distances. For simplicity, we choose equidistant Lorentzians. The resulting level number variance shows the expected overshoot, as displayed in Fig. 15. We can draw an interesting conclusion from this qualitative discussion. In Fig. 16, the fluctuating part $N_{\mathrm{fluc}}(E)$ is shown for the QPM spectra. It is clearly not a simple oscillation as in our qualitative example with the Lorentzians, but it exhibits sizable variations. One is tempted to interpret them as non-statistical variations of the level density due to the presence of doorway-type-of states. If so, this would state a nice confirmation that the QPM calculation catches the physics mechanism in a realistic way. Although we should not overstretch such a conclusion, it is worthwhile to remark that it would be consistent with the findings for all four nuclei.

All in all we are able to construct a consistent interpretation of the observed quantities in the following way: it is rather likely that the $N = 82$ nuclei show a behavior that is in between Poisson and GOE or close to GOE statistics, but different for each nucleus. As we miss at least 90 percent (experiment) or 70 percent (QPM) of the levels, the spectral properties are in any case close to Poisson with some remnants of level repulsion. On the other hand, one would probably not see these remnants of level repulsion in these incomplete sequences, if the full sequences were not correlated. As most of the correlations are lost because of this missing of a large fraction of levels, there is not a big difference between QPM ($f \approx 0.3$) and experiment ($f \approx 0.1$). For the strength distributions the situation is different. These do not contain information about correlations and the loss of the weak transitions—that constitutes a random loss of levels in the spectra—results only in a truncation of the strength distributions below a certain threshold. While the QPM strengths are close to Porter–Thomas statistics, the truncated QPM and the experiment deviate from it. This can be described within the model of Eq. (13) and is shown in Fig. 9. As the distribution of the transition strengths does not allow a direct conclusion on the distribution of the wave function components, it is not very sensitive to the spectral correlations. Thus, it is no contradiction to the spectral statistics found that the distribution of the transition

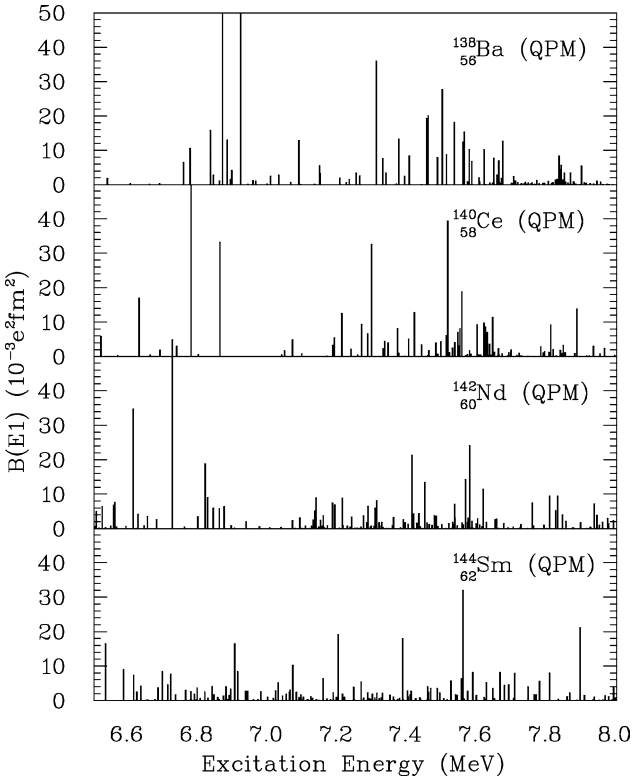


Fig. 14. Enlargement of Fig. 2, where a clustering of the levels can be seen, which leads to the anti-correlation effect observed in the number variances shown in Fig. 8.

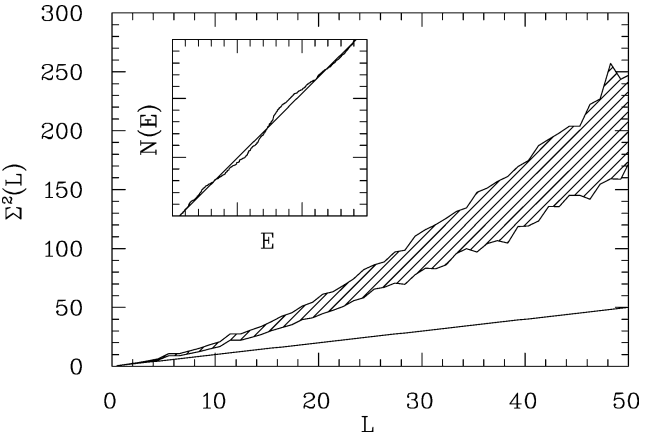


Fig. 15. Number variance for an uncorrelated sequence of random numbers, the density of which has been modified in an oscillating way. As the smooth function fitted to the staircase function (inset) does not take these oscillations into account, the unfolded spectrum shows anti-correlations in the number variance instead of the expected Poisson statistics (full line). This explains the behavior seen in Fig. 8.

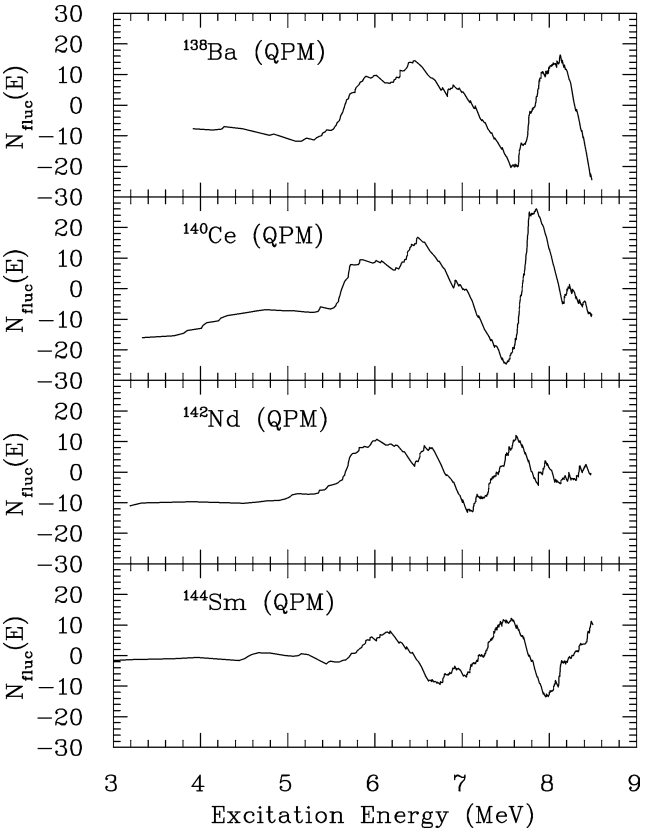


Fig. 16. Spectral fluctuations for the QPM spectra, i.e., $N_{\text{fluc}} = N(E) - N_{\text{av}}(E)$, clarifying that not all of the structure of $N(E)$ is described by the fit of Eq. (7).

strengths is always consistent with a truncated Porter–Thomas distribution. However, we learn from the strengths that experimental and QPM results agree, even though we cannot deduce information about the statistical properties from the strengths.

How do our results fit into the general picture emerging from previous studies [30–36,60] of statistical properties in nuclear spectra? In general, low-lying purely collective excitations show a predominantly uncorrelated behavior as described by Poisson statistics, while non-collective excitations yield a correlated behavior as described by GOE statistics. Famous examples are, on the one hand, the "nuclear data ensemble" [32] of high-lying compound nuclear resonances which show very clean GOE statistics and, on the other hand, high-spin states near the yrast line [34] which yield Poisson behavior. There are naturally also examples where the statistical properties are in between Wigner–Dyson and Poissonian behavior indicating the coexistence between chaotic and regular motion in the nuclear many-body problem. A most recent example for such mixed behavior is provided by the distribution of the ratios of the excitation energies of certain $2^+$ and $4^+$ states in nuclei [36]. The role of the excitation energy is subtle. In the odd–odd nucleus $^{26}$Al, GOE

behavior was found down to the ground state [31]. This proves that the GOE character of the correlations cannot simply be attributed to the energy region in the spectra.

## 7. Conclusion

In summary, we analyzed the statistical properties of E1 excitations in four $N = 82$ nuclei in the energy range between 4 and 8 MeV, the region of the so-called pygmy resonance. The experimental data, although very incomplete, show remnants of spectral correlations. We thus conclude that the full realistic spectra ought to exhibit strong correlations that are GOE-like or close to GOE. In an identical analysis of the statistical properties of E1 strength distributions from a QPM calculation, results are found that are consistent with the experimental findings. In a recent analysis of the magnetic dipole scissors mode in heavy deformed nuclei statistical properties compatible with the Poisson case were found. This provided an independent proof for the collective nature of this particular excitation mechanism [35]. Importantly, these states are very low-lying. The present contribution extends those studies of a particular excitation mechanism into a region of higher excitation energy. As the density of states quickly grows with excitation energy, more states will be available at higher energies to couple to possibly present collective doorway states. This results in correlated spectra, largely independent of the underlying collective or non-collective structure of the mode. Our experimental and theoretical results are consistent with such an interpretation.

## Acknowledgements

We thank S. Volz for providing us with the experimental data sets—in case of $^{142}$Nd even prior to publication—and S. Åberg, O. Bohigas, G.E. Mitchell, and M.P. Pato for useful discussions. A.H. thanks the division of mathematical physics, LTH, Lund University, and A.R. the LPTMS, Orsay, for hospitality during visits where parts of the present work were performed.

## References

[1] G.A. Bartholomew, E.D. Earle, A.J. Ferguson, J.W. Knowles, M.A. Lone, Adv. Nucl. Phys. 7 (1972) 229.
[2] A. Leistenschneider, T. Aumann, K. Boretzky, D. Cortina, J. Cub, U.D. Pramanik, W. Dostal, Th.W. Elze, H. Emling, H. Geissel, A. Grünschloss, M. Hellström, R. Holzmann, S. Ilievski, N. Iwasa, M. Kaspar, A. Kleinbohl, J.V. Kratz, R. Kulessa, Y. Leifels, E. Lubkiewicz, G. Münzenberg, P. Reiter, M. Rejmund, C. Scheidenberger, C. Schlegel, H. Simon, J. Stroth, K. Sümmerer, E. Wajda, W. Walus, S. Wan, Phys. Rev. Lett. 86 (2001) 5442.
[3] E. Tryggestad, T. Aumann, T. Baumann, D. Bazin, J.R. Beene, Y. Blumenfeld, B.A. Brown, M. Chartier, M.L. Halbert, P. Heckman, J.F. Liang, D.C. Radford, D. Shapira, M. Thoennessen, R.L. Varner, Phys. Lett. B 541 (2002) 52;
E. Tryggestad, T. Baumann, P. Heckman, M. Thoennessen, T. Aumann, D. Bazin, Y. Blumenfeld, J.R. Beene, T.A. Lewis, D.C. Radford, D. Shapira, R.L. Varner, M. Chartier, M.L. Halbert, J.F. Liang, Phys. Rev. C 67 (2003) 064309.

[4] S. Nakayama, T. Yamagata, H. Akimune, I. Daito, H. Fujimura, Y. Fujita, M. Fujiwara, K. Fushimi, T. Inomata, H. Kohri, N. Koori, K. Takahisa, A. Tamii, M. Tanaka, H. Toyokawa, Phys. Rev. Lett. 85 (2000) 262.
[5] K. Langanke, M. Wiescher, Rep. Prog. Phys. 64 (2001) 1657.
[6] S. Goriely, Phys. Lett. B 436 (1998) 10.
[7] O. Bohigas, N. Van Giai, D. Vautherin, Phys. Lett. B 102 (1981) 105.
[8] R. Mohan, M. Danos, L.C. Biedenharn, Phys. Rev. C 3 (1971) 1740.
[9] Y. Suzuki, K. Ikeda, H. Sato, Prog. Theor. Phys. 83 (1990) 180.
[10] P. Van Isacker, M.A. Nagarajan, D.D. Warner, Phys. Rev. C 45 (1992) R13.
[11] J. Chambers, E. Zaremba, J.P. Adams, B. Castel, Phys. Rev. C 50 (1994) R2671.
[12] J.P. Adams, B. Castel, H. Sagawa, Phys. Rev. C 53 (1996) 1016.
[13] S.I. Bastrukov, S. Misiçu, A.V. Sushkov, Nucl. Phys. A 562 (1993) 191.
[14] E.B. Balbutsev, I.V. Molodtsova, A.V. Unzhakova, Europhys. Lett. 26 (1994) 499.
[15] S. Misiçu, S.I. Bastrukov, Eur. Phys. J. A 13 (2002) 399.
[16] F. Iachello, Phys. Lett. B 160 (1985) 1.
[17] A.M. Oros, K. Heyde, C. De Coster, B. Decroix, Phys. Rev. C 57 (1998) 990.
[18] G. Colò, N. Van Giai, P.F. Bortignon, M.R. Quaglia, Phys. Lett. B 485 (2000) 362.
[19] D. Vretenar, A. Wandelt, P. Ring, Phys. Lett. B 487 (2000) 334.
[20] J. Piekarewicz, Phys. Rev. C 64 (2001) 024307.
[21] D. Vretenar, N. Paar, P. Ring, G.A. Lalazissis, Phys. Rev. C 63 (2001) 047301.
[22] N. Ryezayeva, T. Hartmann, Y. Kalmykov, H. Lenske, P. von Neumann-Cosel, V.Yu. Ponomarev, A. Richter, A. Shevchenko, S. Volz, J. Wambach, Phys. Rev. Lett. 89 (2002) 272502.
[23] R.-D. Herzberg, P. von Brentano, J. Eberth, J. Enders, R. Fischer, N. Huxel, T. Klemme, P. von Neumann-Cosel, N. Nicolay, N. Pietralla, V.Yu. Ponomarev, J. Reif, A. Richter, C. Schlegel, R. Schwengner, S. Skoda, H.G. Thomas, I. Wiedenhöver, G. Winter, A. Zilges, Phys. Lett. B 390 (1997) 49.
[24] R.-D. Herzberg, C. Fransen, P. von Brentano, J. Eberth, J. Enders, A. Fitzler, L. Käubler, H. Kaiser, P. von Neumann-Cosel, N. Pietralla, V.Yu. Ponomarev, H. Prade, A. Richter, H. Schnare, R. Schwengner, S. Skoda, H.G. Thomas, H. Tiesler, D. Weisshaar, I. Wiedenhöver, Phys. Rev. C 60 (1999) 051307(R).
[25] H. Sagawa, T. Suzuki, Phys. Rev. C 59 (1999) 3116.
[26] C. Colò, P.F. Bortignon, Nucl. Phys. A 696 (2001) 427.
[27] T. Hartmann, J. Enders, P. Mohr, K. Vogt, S. Volz, A. Zilges, Phys. Rev. Lett. 85 (2000) 274;
T. Hartmann, J. Enders, P. Mohr, K. Vogt, S. Volz, A. Zilges, Phys. Rev. C 65 (2002) 034301.
[28] A. Zilges, S. Volz, M. Babilon, T. Hartmann, P. Mohr, K. Vogt, Phys. Lett. B 542 (2002) 43.
[29] D. Vretenar, N. Paar, P. Ring, T. Niksic, Phys. Rev. C 65 (2002) 021301.
[30] T. Guhr, A. Müller-Groeling, H.A. Weidenmüller, Phys. Rep. 299 (1998) 189.
[31] G.E. Mitchell, E.G. Bilpuch, P.M. Endt, J.F. Shriner Jr., Phys. Rev. Lett. 61 (1988) 1473.
[32] R.U. Haq, A. Pandey, O. Bohigas, Phys. Rev. Lett. 48 (1982) 1086.
[33] J.F. Shriner Jr., G.E. Mitchell, T. von Egidy, Z. Phys. A 338 (1991) 309.
[34] J.D. Garrett, J.Q. Robinson, A.J. Foglia, H.Q. Jin, Phys. Lett. B 392 (1997) 24.
[35] J. Enders, T. Guhr, N. Huxel, P. von Neumann-Cosel, C. Rangacharyulu, A. Richter, Phys. Lett. B 486 (2000) 273.
[36] A.Y. Abul-Magd, H.L. Harney, M.H. Simbel, H.A. Weidenmüller, Phys. Lett. B 579 (2004) 278.
[37] S. Volz, et al., in preparation.
[38] P. Mohr, J. Enders, T. Hartmann, H. Kaiser, D. Schiesser, S. Schmitt, S. Volz, F. Wissel, A. Zilges, Nucl. Instrum. Methods A 423 (1999) 480.
[39] A. Richter, in: S. Myers, et al. (Eds.), Proceedings 5th European Particle Accelerator Conference, Sitges, Spain, 1996, IOP, Bristol, 1996, p. 110.
[40] R.-D. Herzberg, I. Bauske, P. von Brentano, T. Eckert, R. Fischer, W. Geiger, U. Kneissl, J. Margraf, H. Maser, N. Pietralla, H.H. Pitz, A. Zilges, Nucl. Phys. A 592 (1995) 211.
[41] F.R. Metzger, Prog. Nucl. Phys. 7 (1959) 53.
[42] U. Kneissl, H.H. Pitz, A. Zilges, Prog. Part. Nucl. Phys. 38 (1996) 349.
[43] C. Hutter, M. Babilon, W. Bayer, D. Galaviz, T. Hartmann, P. Mohr, S. Müller, W. Rochow, D. Savran, K. Sonnabend, K. Vogt, S. Volz, A. Zilges, Nucl. Instrum. Methods A 489 (2002) 247.

[44] N. Pietralla, Z. Berant, V.N. Litvinenko, S. Hartman, F.F. Mikhailov, I.V. Pinayev, G. Swift, M.W. Ahmed, J.H. Kelley, S.O. Nelson, R. Prior, K. Savourov, A.P. Tonchev, H. Weller, Phys. Rev. Lett. 88 (2002) 012502.
[45] V.G. Soloviev, Theory of Atomic Nuclei: Quasiparticles and Phonons, IOP, Bristol, 1992.
[46] C.A. Bertulani, V.Yu. Ponomarev, Phys. Rep. 321 (1999) 139.
[47] M.L. Mehta, Random Matrices, second ed., Academic Press, San Diego, 1991.
[48] C.E. Porter, Statistical Theories of Spectra: Fluctuations, Academic Press, New York, 1965.
[49] O. Bohigas, in: M.J. Gianonni, A. Voros, J. Zinn-Justin (Eds.), Chaos and Quantum Physics, Elsevier, Amsterdam, 1991.
[50] A.A. Adams, G.E. Mitchell, W.E. Ormand, J.F. Shriner Jr., Phys. Lett. B 392 (1997) 1.
[51] C. Dembowski, H.-D. Gräf, A. Heine, H. Rehfeld, A. Richter, C. Schmit, Phys. Rev. E 62 (2000) R4516.
[52] A. Delon, R. Jost, M. Lombardi, J. Chem. Phys. 95 (1991) 5701.
[53] H.P. Baltes, E.R. Hilf, Spectra of Finite Systems, Bibliographisches Institut, Mannheim, 1976.
[54] U. Agvaanluvsan, G.E. Mitchell, J.F. Shriner Jr., M.P. Pato, Nucl. Instrum. Methods A 498 (2003) 459.
[55] O. Bohigas, M.P. Pato, Phys. Lett. B, submitted for publication.
[56] C.I. Barbosa, T. Guhr, H.L. Harney, Phys. Rev. E 62 (2000) 1936.
[57] T.A. Brody, J. Flores, J.B. French, P.A. Mello, A. Pandey, S.S.M. Wong, Rev. Mod. Phys. 53 (1981) 385.
[58] O. Bohigas, S. Tomsovic, D. Ullmo, Phys. Rep. 223 (1993) 43.
[59] F.H. Fröhner, in: Course on Nuclear Theory for Applications, IAEA Report No. IAEA-SMR-43, p. 58.
[60] M. Matsuo, T. Døssing, E. Vigezzi, S. Åberg, Nucl. Phys. A 620 (1997) 296.